Macromolecules
ARTICLE

Macromolecules **2010**, *43*, 6953–6961 **6953**
DOI: 10.1021/ma100785m

Core−Shell Dendriplexes with Sterically Induced Stoichiometry for Gene Delivery

Manuela Raviña,[†] Maria de la Fuente,[†] Juan Correa,[‡] Ana Sousa-Herves,[‡] Jorge Pinto,[†] Eduardo Fernandez-Megia,*[,‡] Ricardo Riguera,[‡] Alejandro Sanchez,[†] and Maria Jose Alonso*[,†]

[†]*Department of Pharmacy and Pharmaceutical Technology, University of Santiago de Compostela, 15782 Santiago de Compostela, Spain, and* [‡]*Department of Organic Chemistry and Center for Research in Biological Chemistry and Molecular Materials, University of Santiago de Compostela, Jenaro de la Fuente s/n, 15782 Santiago de Compostela, Spain*

Received April 10, 2010; Revised Manuscript Received July 13, 2010

ABSTRACT: The development of dendriplexes as nanoarchitectures with sterically induced stoichiometry for gene delivery applications is described. The ability of four generations of amino-functionalized gallic acid−triethylene glycol (GATG) dendrons and PEG−dendritic block copolymers to efficiently condense pDNA was evaluated. A characteristic nitrogen to phosphate ratio (N/P) for complete pDNA condensation was revealed for each dendrimer. Larger N/P ratios had little effect on the size and ξ potential of the dendriplexes. Dendriplexes are envisioned as core−shell nanostructures, where the relative size between the condensed pDNA at the core and the shell dendrimers limits the core−shell stoichiometry by steric reasons. By application of the Mansfield−Tomalia−Rakesh equation, a 3-fold reduction in the number of shell dendrimers has been estimated on increasing the dendrimer generation one unit. Overall, the dendritic architecture (generation and PEGylation) determines the properties of the dendriplexes, offering a great opportunity for fine-tuning the requirements for specific gene therapy applications.

Introduction

Gene therapy is a branch of molecular medicine that has the potential to significantly impact human health in this century by providing new treatments for a large number of inherited and acquired diseases. The basic concept of gene therapy is to introduce a piece of genetic material into target cells with the aim of curing or slowing the progression of a disease. To achieve this goal, gene therapy requires technologies capable of delivering genes into a wide variety of cells, tissues, and organs. Although the first delivery systems tested were based on modified viruses, safety concerns have led to a careful reconsideration of their application for human clinical trials and prompted the development of synthetic vectors.[1] Among them, dendrimers are especially appealing because of their monodisperse and globular structure, the presence of a large number of peripheral groups, and their stepwise preparation through generations with discrete properties.[2−8] The commercial availability and relative efficiency of poly(amidoamine) (PAMAM) and poly(propyleneimine) (PPI) dendrimers have resulted in these materials and their derivatives currently dominating the area of gene delivery with dendrimers.[9,10] In addition, alternative dendritic structures, such as those based on poly(L-lysine) (PLL)[11] and amphiphilic dendritic vectors, have also been investigated.[12]

Similarly to dendrimers, dendritic wedges, also known as dendrons, have been successfully used in gene delivery.[13] The possibility of differently and selectively functionalizing the focal point and the periphery of dendrons to incorporate polymers, targeting/imaging agents, probes, and ligands has been proposed for drug delivery and other biomedical applications.[14−19] In this context, we have recently described the preparation of a new family of azide-terminated dendrons and their block copolymers with poly(ethylene glycol) ([G*n*]-N_3 and PEG-[G*n*]-N_3, where *n* is the generation number) that comprise a gallic acid core and triethylene glycol spacer arms (gallic acid−triethylene glycol dendrimers, GATG, Figure 1).[20,21] GATG dendrimers benefit from an easy structural modification and an adequate aqueous solubility and biocompatibility due to the presence of the ethylene glycol arms. The peripheral azides in GATG dendrimers have been exploited in the context of click chemistry for the preparation of glyco- and anionic-dendrimers, interesting tools in the study of the multivalent carbohydrate−receptor interaction and

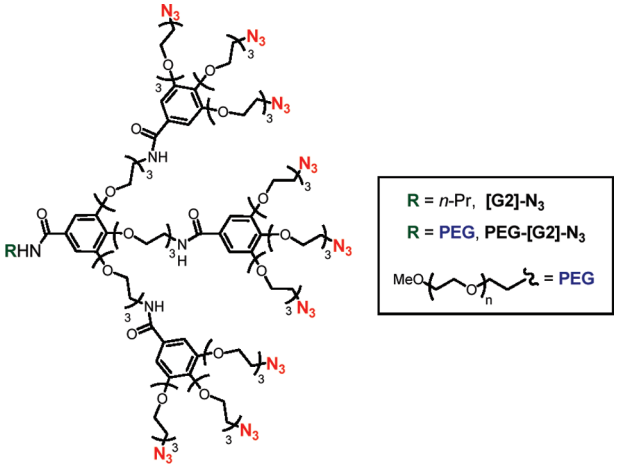

Figure 1. Representative structure of GATG dendrimers: [G2]-N_3 and PEG-[G2]-N_3.

*Corresponding authors: Tel + 34 981 594627, Fax + 34 981 547148, e-mail mariaj.alonso@usc.es (M.J.A.); e-mail ef.megia@usc.es (E.F.-M.).

Published on Web 08/06/2010

the dynamics of dendrimers, and the preparation of stable polyion complex micelles.[22−24]

Taking into account the excellent opportunities brought about by dendrimers in gene delivery,[2−8] we decided to explore the utility of the GATG family in this field. In our opinion, GATG dendrimers fulfill many of the structural demands for an efficient gene transfection. Thus, by reduction of the terminal azides, amine-decorated dendrimers would result with a high positive charge in physiological media and thus the ability to condense and protect nucleic acids. In addition, the hydrophobic nature of gallic acid is expected to enhance the transfection efficiency of the resulting dendriplexes by modulating complex interactions with cells, such as adsorption and cellular uptake. Indeed, it has been reported that the incorporation of hydrophobic units within the structure of polycationic vectors facilitates the destabilization of the endosomal membrane, increasing transfection. For example, PEI,[25] PLL,[26] and PAMAM[27,28] dendrimers showed higher transfection efficiencies when hydrophobically modified with cholesterol or fatty acids. Moreover, polyplexes relying on hydrophobic as well as electrostatic interactions have been reported to more easily release DNA after internalization.[29]

A main drawback of polymeric gene delivery vectors is their rapid clearance from the plasma following intravenous administration due to aggregation with blood components. In addition, the high charge density of the resulting dendriplexes usually renders them cytotoxic and therefore of limited utility for in vivo applications. Consequently, in order to move from a simple nucleic acid transport in vitro to gene therapy in vivo, stable vectors in biological fluids are required. A common strategy for this goal has traditionally been the shielding of the charge at the surface with hydrophilic polymers such as PEG. The resulting stealth vectors are characterized by lower toxicities, enhanced solubilities, and longer circulation times in vivo.[30−36] In the case of the GATG family, the presence of biocompatible triethylene glycol spacer arms and the easy functionalization of the focal point with PEG are envisioned as sources of steric stabilization for the resulting dendriplexes.

Herein, we report our initial results on the development of GATG dendrimers as a novel gene delivery platform. To this end, amino-functionalized dendrons and PEG−dendritic block copolymers of generations 1−4 (G1−G4) were synthesized, and their complexation with a plasmid DNA (pDNA) was studied. Moreover, the biophysical characterization of the resulting dendriplexes is presented. By studying the structural properties of the dendriplexes, we seek to understand the effect of generation and presence/absence of PEG on the pDNA−dendrimer interaction in terms of binding capacity, dendriplex size, surface charge, and morphology.

Experimental Section

1. Materials and General Methods. PEG−dendritic block copolymers have been synthesized starting from a commercially available (Fluka) MeO−PEG−OH (M_n 5055.5, M_w 5087.8 by MALDI-TOF). Polydispersity index (PDI) of PEG-[G*n*]-N_3: PEG-[G1]-N_3 (1.004), PEG-[G2]-N_3 (1.002), and PEG-[G3]-N_3 (1.032), as determined by MALDI-TOF.[20,21] NMR chemical shifts are reported in ppm (δ units) downfield from internal tetramethylsilane ($CDCl_3$) or the HOD signal (D_2O). Ultrafiltration was performed on Amicon stirred cells with Amicon YM membranes. pDNA encoding green fluorescent protein (pEGFP-C1) driven by a CMV promoter was purchased from Elim Biopharmaceuticals (San Francisco, CA). Trizma base, agarose, xylene cyanole, bromophenol blue, and ethidium bromide (purity 95%) were all obtained from Sigma-Aldrich (Madrid, Spain). 1 kbp DNA ladder was obtained from Life Technologies (Barcelona, Spain). All other solvents and chemicals were of the highest grade commercially available.

2. Synthesis of GATG Dendrimers. *2.1.* [*G3*]-*NH_2*. Pd/C (10 mg, 20%) was added to a degassed (Ar) solution of [G3]-N_3 (50 mg, 6.3 μmol) in MeOH:EtOAc (3:1, 2.0 mL). The flask was purged with Ar and then evacuated (vacuum) and pressurized (H_2, 1 atm) three times. HCl (0.114 mL, 0.342 mmol, 3 M) was added, and the resulting mixture was stirred under H_2 (1 atm) for 24 h. Then, the catalyst was removed by filtration through Celite, and the filtrate was concentrated to give the hydrochloride salt of [G3]-NH_2 as a pale yellow oil (51 mg, 99%). ^{1}H NMR (400 MHz, D_2O) δ: 7.20−6.98 (m, 26H), 4.38−3.48 (m, 414H), 3.45−3.38 (m, 2H), 3.30−3.15 (m, 54H), 1.64−1.43 (m, 2H), 0.9 (t, J = 6.6 Hz, 3H). ^{13}C NMR (100 MHz, D_2O) δ: 170.2, 152.8, 140.5, 130.5, 107.3, 106.2, 73.1, 71.1, 70.8, 70.6, 70.1, 69.9, 69.3, 69.2, 67.4, 40.9, 40.1, 29.3, 21.9, 11.2. IR (KBr, cm^{-1}): 2931, 2876, 1708, 1636, 1581, 1495, 1136.

2.2. [*G4*]-*N_3*. Pd/C (20 mg, 20%) was added to a degassed (Ar) solution of [G3]-N_3 (100 mg, 12.7 μmol) in MeOH:EtOAc (3:1, 2.0 mL). The flask was purged with Ar and then evacuated (vacuum) and pressurized (H_2, 1 atm) three times. The resulting mixture was stirred under H_2 (1 atm) for 24 h. Then, the catalyst was removed by filtration through Celite, and the filtrate was concentrated to give [G3]-NH_2. HOBt (132 mg, 0.687 mmol) and EDC·HCl (93 mg, 0.687 mmol) were added to a solution of the above residue and 3,4,5-tri-(2-(2-(2-azidoethoxy)ethoxy)-ethyl)benzoic acid[21] (440 mg, 0,687 mmol) in DMSO (2 mL). Reaction was allowed to stir at rt for 48 h under Ar and then was concentrated. The resulting crude product was ultrafiltered (Amicon YM3, MeOH:^{i}PrOH:DMSO, 1:1:0.2) to afford pure [G4]-N_3 (265 mg, 87%) as a yellow oil. ^{1}H NMR (400 MHz, $CDCl_3$) δ: 7.25−7.05 (m, 80H), 4.34−4.02 (m, 480H), 3.98−3.46 (m, 960H), 3.45−3.23 (m, 164H), 1.65−1.48 (m, 2H), 0.87 (br s, 3H). ^{13}C NMR (75 MHz, $CDCl_3$) δ: 167.0, 142.4, 141.3, 129.6, 107.0, 72.3, 70.8, 70.7, 70.6, 70.5, 70.2, 70.0, 69.9, 69.7, 69.0, 50.6, 39.9, 29.6, 22.6, 14.0. IR (KBr, cm^{-1}): 3294, 2926, 2871, 2105, 1718, 1651, 1583, 1120.

2.3. [*G4*]-*NH_2*. Pd/C (10 mg, 20%) was added to a degassed (Ar) solution of [G4]-N_3 (89 mg, 3.5 μmol) in MeOH:AcOEt (1:1, 2.0 mL). The flask was purged with Ar and then evacuated (vacuum) and pressurized (H_2, 1 atm) three times. HCl (0.156 mL, 0.468 mmol, 3 M) was added, and the resulting mixture was stirred under H_2 (1 atm) for 24 h. Then, the catalyst was removed by filtration through Celite, and the filtrate was concentrated to give the hydrochloride salt of [G4]-NH_2 as a pale yellow oil (82 mg 90%). ^{1}H NMR (250 MHz, D_2O) δ: 7.17−6.90 (m, 80H), 4.30−3.24 (m, 1440H), 3.22−3.04 (m, 164H), 1.58−1.45 (m, 2H), 0.81 (br s, 3H).

2.4. *PEG*-[*G3*]-*NH_2*. Pd/C (60 mg, 20%) was added to a degassed (Ar) solution of PEG-[G3]-N_3 (300 mg, 23 μmol) in MeOH (2.3 mL). The flask was purged with Ar and then evacuated (vacuum) and pressurized (H_2, 1 atm) three times. HCl (0.345 mL, 1.035 mmol, 3 M) was added, and the resulting mixture was stirred under H_2 (1 atm) for 24 h. Then, the catalyst was removed by filtration through Celite washing with MeOH, and the filtrate was concentrated and freeze-dried to give the hydrochloride salt of PEG-[G3]-NH_2 as a white foam (284 mg, 93%). ^{1}H NMR (400 MHz, D_2O) δ: 7.18−7.09 (m, 26H), 4.37−4.04 (m, 80H), 3.99−3.48 (m, ∼966H), 3.41 (s, 3H), 3.27−3.19 (m, 56H). ^{13}C NMR (100 MHz, D_2O) δ: 171.3, 154.0, 141.7, 131.7, 108.5, 74.3, 73.9, 73.2, 73.0, 72.3, 72.0, 71.8, 71.3, 71.1, 70.6, 70.4, 68.6, 41.8, 41.3. IR (KBr, cm^{-1}): 2875, 1496, 1344, 1112.

2.5. *PEG*-[*G4*]-*N_3*. The hydrochloride salt of PEG-[G3]-NH_2 (50 mg, 3.76 μmol) and 3,4,5-tri-(2-(2-(2-azidoethoxy)ethoxy)-ethyl)benzoic acid[21](131 mg, 0.204 mmol) were dissolved in CH_2Cl_2 (380 μL) and Et_3N (28 μL). HOBt (28 mg, 0.204 mmol) and EDC·HCl (39 mg, 0.204 mmol) were added, and the resulting solution was stirred at rt for 48 h under Ar. Then, the reaction was concentrated and precipitated twice from MeOH:^{i}PrOH and CH_2Cl_2:Et_2O to give pure PEG-[G4]-N_3 (95 mg, 87%). ^{1}H NMR (400 MHz, $CDCl_3$) δ: 7.21−7.03 (m, 80H),

4.30−4.03 (m, 242H), 3.94−3.43 (m, 1614H), 3.40−3.27 (m, 167H). ^{13}C NMR (100 MHz, $CDCl_3$) δ: 167.0, 152.3, 152.2, 141.1, 129.6, 109.1, 106.8, 72.3, 70.8, 70.7, 70.6, 70.4, 70.3, 70.1, 69.7, 69.5, 68.9, 68.8, 50.6, 39.9. IR (KBr, cm^{-1}): 2871, 2105, 1495, 1331, 1117.

2.6. PEG-[G4]-NH_2. Pd/C (14 mg, 20%) was added to a degassed (Ar) solution of PEG-[G4]-N_3 (70 mg, 2.4 μmol) in MeOH:THF (2:1, 3.0 mL). The flask was purged with Ar and then evacuated (vacuum) and pressurized (H_2, 1 atm) three times. HCl (0.108 mL, 0.324 mmol, 3 M) was added, and the resulting mixture was stirred under H_2 (1 atm) for 24 h. Then, the catalyst was removed by filtration through Celite washing with MeOH, and the filtrate was concentrated and freeze-dried to give the hydrochloride salt of PEG-[G4]-NH_2 as a pale foam (63 mg, 89%). ^{1}H NMR (400 MHz, $CDCl_3$) δ: 7.20−7.02 (m, 80H), 4.40−4.01 (m, 242H), 3.94−3.48 (m, 1614H), 3.42 (s, 3H), 3.35−3.18 (m, 164H). ^{13}C NMR (100 MHz, $CDCl_3$) δ: 167.4, 153.0, 140.9, 129.4, 107.7, 72.4, 70.6, 70.1, 69.4, 40.1. IR (CsI, cm^{-1}): 2873, 1496, 1333, 1106.

3. Dendriplex Formation. Dendriplexes were formulated at different charge ratios (N/P) from 1/1 to 40/1. The charge ratio was defined as the ratio between the maximum number of protonable primary amines in the dendrimers and the number of negative phosphates in pDNA.[37] For dendriplex formation, an aqueous solution of the dendrimer (240 μL) was added to a pDNA solution in 50 mM HEPES buffer pH 7.4 (40 μL) and mixed by vigorous pipetting. The dendriplexes were allowed to stabilize for at least 20 min at rt before use. pDNA concentration was maintained at 25 μg/mL. Dendrimer concentration was varied in order to achieve the desired charge ratio (N/P).

4. Agarose Gel Electrophoresis and pDNA Condensation Assay. Agarose gel electrophoresis: Dendriplexes (30 μL) at different N/P charge ratios from 1/1 to 40/1 were electrophoresed on a 1% agarose gel containing ethidium bromide (EB, 0.5 μg/mL) and analyzed by UV to show the location of pDNA. Electrophoresis was performed at a voltage of 75 V for 1 h in TAE running buffer.

DNA condensation assay: DNA condensation was measured by fluorescence of complex solutions upon addition of EB.[38] Dendriplexes were placed on 96 well plates and incubated with EB (5 μg/mL). The total amount of DNA per well was 0.6 μg. The plate was then analyzed on a Perkin-Elmer LS 50 B fluorescence plate reader with excitation wavelength at 330 nm and emission at 600 nm. The maximum fluorescence signal was obtained when EB was incubated with naked DNA.

5. Measurement of Dendriplex Size and ζ-Potential. The mean particle size of the dendriplexes was determined by photon correlation spectroscopy (PCS). Each analysis was carried out at 25 °C with an angle detection of 90° (Zetasizer 3000 HS, Malvern Instruments, England). ζ-potential values of the dendriplexes were obtained by laser doppler anemometry (LDA), measuring the mean electrophoretic mobility (Zetasizer Nano-series Nano-ZS, Malvern Instruments, England). Measurements were performed in 1 mM KCl.

6. Translational Diffusion Data of [G*n*]-NH_2. ^{1}H pulsed field-gradient (PFG) NMR experiments of the hydrochloride salts of [G2]-NH_2 and [G3]-NH_2 were acquired in D_2O using a Varian INOVA 750 MHz spectrometer equipped with a triple gradient shielded probe at 298 K. The pulse sequence used includes bipolar-gradient pulse pairs and a stimulated echo with an additional delay time for longitudinal eddy current compensation (LED-BPPSTE).[39] The diffusion coefficients (D_t) were determined using the Stejskal−Tanner equation (Figure 2). Linear fits of the echo intensities (A) were plotted on a natural log scale vs $\gamma^2\delta^2g^2(\Delta - \delta/3)$, where γ is the magnetogyric ratio of the ^{1}H nucleus, δ is the length of the gradient pulse, g is the gradient strength, and Δ is the time separation between gradient pulses. The gradient was varied linearly along 16 experiments from 2 to 65 G cm^{-1} to obtain the diffusion data. The gradient strengths were calibrated measuring the diffusion of residual protons in D_2O (2.22×10^{-9} m^2 s^{-1} at 298 K).[40] Experiments were realized in triplicate at concentrations 0.2 and 0.3 g/L with a Δ of 250 ms. The duration of the gradients in the sequence was set at 1 ms followed by a stabilization delay period of 0.2 ms. The recovery delay was 10 s. The number of scans used was 64. Similar experiments were recorded for [G3]-NH_2 (0.3 g/L, 128 scans) at varying diffusion times Δ (100, 250, and 400 ms) (Figure 3). Since D_t remained constant in the range of concentrations studied, and experiments with varying diffusion times Δ rendered identical spin-echo decays, it was concluded dendrimers being under extremely dilute conditions and thus diffusion entirely dependent on size ($D_t \sim D_0$, diffusion coefficient at zero polymer concentration) (Table 1). From the D_0 values, the hydrodynamic radii (R_h) of [G2]-NH_2 and [G3]-NH_2 were estimated by using the Stokes−Einstein equation (Table 1).

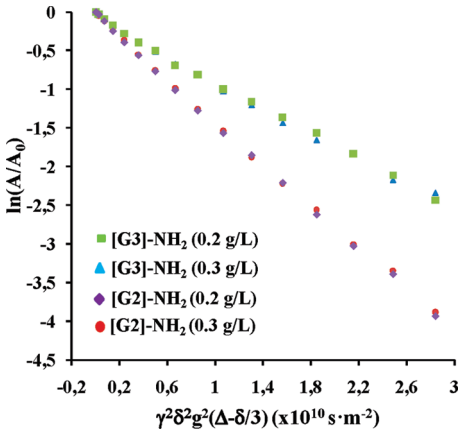

Figure 2. Determination of diffusion coefficients (D_t) for [G2]-NH_2 and [G3]-NH_2 (0.2 and 0.3 g/L in D_2O) by means of Stejskal−Tanner plots.

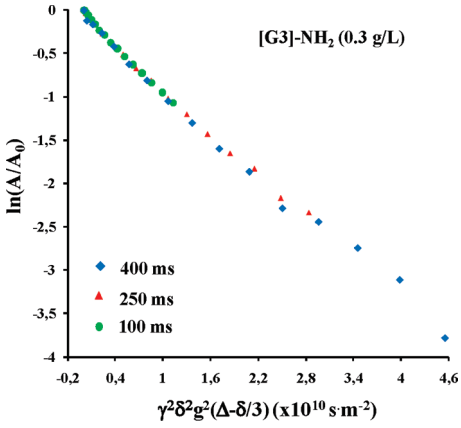

Figure 3. Stejskal−Tanner plots of [G3]-NH_2 (0.3 g/L in D_2O) at varying diffusion times (Δ): 100, 250, and 400 ms.

Table 1. D_0 ($\times 10^{-10}$ m^2 s^{-1}) and R_h (nm) for [G*n*]-NH_2

	[G2]-NH_2	[G3]-NH_2
D_0 (0.3 g/L)[a]	1.34 (0.03)	0.837 (0.01)
R_h[a]	1.49 (0.03)	2.38 (0.03)

[a] Standard deviation shown in parentheses.

7. Atomic Force Microscopy (AFM). For AFM measurements, dendriplexes were diluted in H_2O to a final concentration in pDNA of 10 μg/mL. Aliquots (1 μL) of the dendriplex solutions were placed on a freshly cleaved untreated mica surface and allowed to stick for 1−2 min. Excess solution was removed by careful absorption onto filter paper. The mica surface was further dried at room temperature for 24 h. Images

Scheme 1

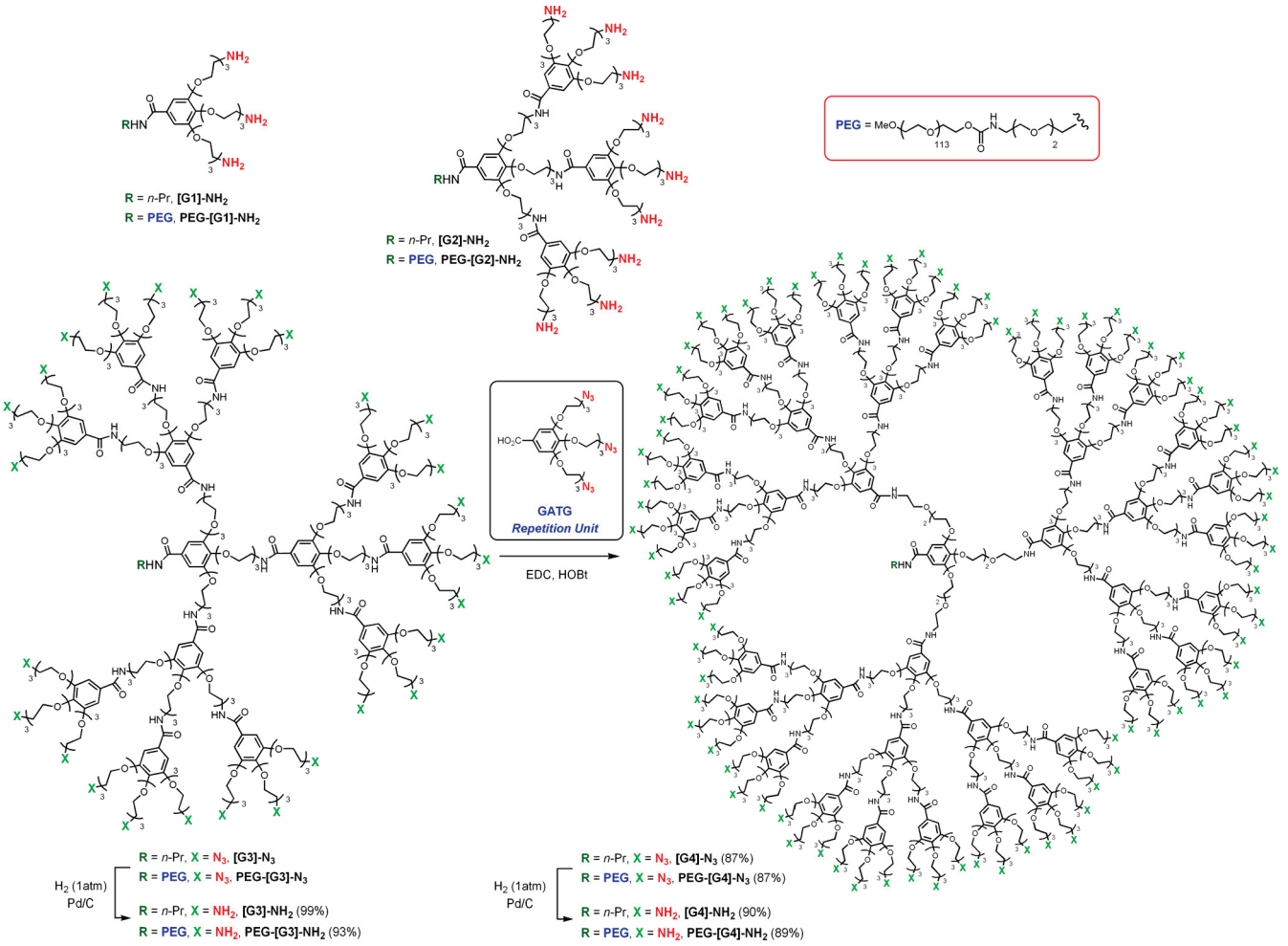

were acquired with a Nanotec SPM (scanning probe microscopy) using tapping mode.

8. Transmision Electron Microscopy (TEM). The morphological evaluation of the dendriplexes was performed by transmission electron microscopy (CM 12 Philips, Eindhoven, The Netherlands). Samples were stained with 2% w/v phosphotungstic acid, on copper grids with Formvar, and dried overnight before analysis.

Results and Discussion

1. Synthesis of GATG Dendrimers. Azide-terminated GATG dendrons and PEG−dendritic block copolymers ([G*n*]-N_3 and PEG-[G*n*]-N_3) were divergently synthesized from 3,4,5-tri-(2-(2-(2-azidoethoxy)ethoxy)ethyl)benzoic acid and propylamine (*n*-PrNH_2) or an amino-terminated PEG-5000 (Scheme 1).[20,21,23] The reduction of the terminal azides in these structures renders amino-terminated dendrimers ([G*n*]-NH_2 and PEG-[G*n*]-NH_2) with a high positive charge at physiological pH and hence the capability to condensate nucleic acids. The preparation of the two first generations of these amino-terminated dendrimers has been previously described by our group.[20,21] We report herein the synthesis of the G3 and G4 for the first time (Scheme 1 and Table 2). More specifically, catalytic hydrogenation of [G3]-N_3 and PEG-[G3]-N_3 [H_2 (1 atm), Pd/C (20%)] led to [G3]-NH_2 and PEG-[G3]-NH_2 in excellent yields (99 and 93%, respectively). In both cases, the completeness of the reduction was monitored by ^{1}H and ^{13}C NMR spectroscopy (D_2O) by the disappearance of the signals of the methylenes adjacent to the azide groups (3.4 ppm in ^{1}H NMR, 50 ppm in ^{13}C NMR) and the appearance of characterisctic signals of methylenes adjacent to protonated amino groups (3.2 ppm in ^{1}H NMR, 40 ppm in ^{13}C NMR).[20,21,23]

Table 2. Molecular Weight (MW) and Number of Peripheral Amino Groups in GATG Dendrimers

dendrimer[a]	calculated MW[b]	amino groups
[G1]-NH_2	604.7	3
[G2]-NH_2	2241.6	9
[G3]-NH_2	7152.2	27
[G4]-NH_2	21884.0	81
PEG-[G1]-NH_2	5764.9	3
PEG-[G2]-NH_2	7401.8	9
PEG-[G3]-NH_2	12312.4	27
PEG-[G4]-NH_2	27044.2	81

[a] PEG−dendritic block copolymers were synthesized from a MeO-PEG-NH_2 with M_n 5219.3 and M_w 5241.9 by MALDI-TOF. [b] M_n in the case of PEG−dendritic block copolymers.

For the syntheses of the amino-functionalized dendrimers of G4, [G3]-NH_2 and PEG-[G3]-NH_2 were treated with the GATG repetition unit under amide coupling conditions (EDC, HOBt, Scheme 1). Once the reactions were completed, crude [G4]-N_3 was purified by ultrafiltration and PEG-[G4]-N_3 by precipitation (MeOH/iPrOH). In this way, the expected G4 azide-terminated dendrimers were obtained in very good yields (87%). Hydrogenation of these materials under similar conditions to those reported above led to [G4]-NH_2 and PEG-[G4]-NH_2 in very good yields (89−90%). Again, the progress of the dendritic generation growth and

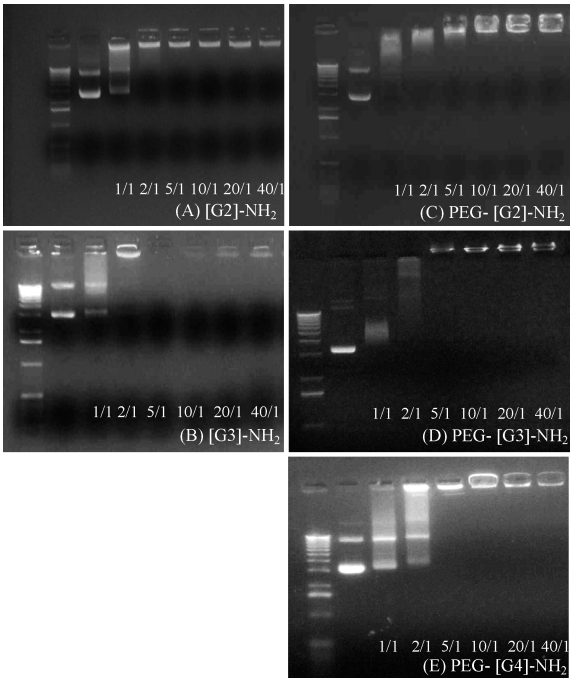

Figure 4. Agarose gel electrophoresis of the dendriplexes from GATG dendrimers and pDNA: [G2]-NH_2 (A), [G3]-NH_2 (B), PEG-[G2]-NH_2 (C), PEG-[G3]-NH_2 (D), PEG-[G4]-NH_2 (E). Charge ratios (N/P) are indicated below each lane. In all cases, column 1 corresponds to a DNA ladder and column 2 to naked pDNA.

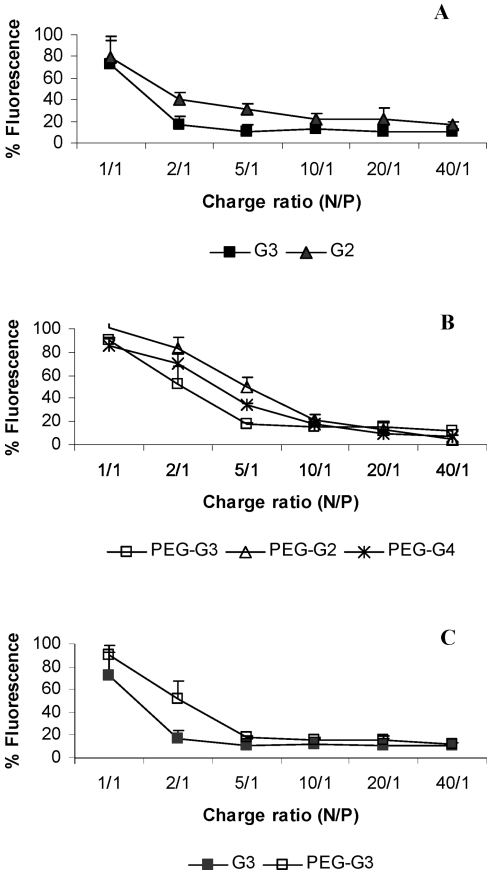

Figure 5. Ethidium bromide fluorescence assay for dendriplexes: (A) [G2]-NH_2 and [G3]-NH_2; (B) PEG-[G2]-NH_2, PEG-[G3]-NH_2, and PEG-[G4]-NH_2; (C) [G3]-NH_2 and PEG-[G3]-NH_2.

hydrogenation processes was easily monitored by ^1H and ^{13}C NMR thanks to the characteristic signals of the methylenes adjacent to the amino and azide groups.[20,21,23]

2. pDNA Binding Ability of GATG Dendrimers. The ability of GATG dendrimers [G*n*]-NH_2 and PEG-[G*n*]-NH_2 of generations G1−G4 to form dendriplexes with a pDNA was examined by agarose gel electrophoresis and ethidium bromide (EB) fluorescence assay. It was seen that [G1]-NH_2 and PEG-[G1]-NH_2 were not capable of inhibiting the migration of the pDNA in an electrophoresis gel, reflecting their failure to efficiently associate pDNA in agreement with previous reports for PAMAM, PLL, and PPI dendrimers.[9−11] For higher generations, the amount of free pDNA able to migrate in the gel decreased as increasing amounts of GATG dendrimers were added (Figure 4). Unfortunately, the limited solubility of [G4]-NH_2 led to discontinue the study with this dendrimer.

These results were corroborated by an EB fluorescence assay (Figure 5). EB is a cationic dye that after intercalation into DNA leads to a significant fluorescence enhancement,[41] which is inhibited when DNA is condensed into particles. Figure 5 shows that PEGylated and non-PEGylated G2 and G3 dendrimers and PEG-[G4]-NH_2 were capable of inhibiting EB intercalation into pDNA.

As expected, the amount of dendrimer necessary for complete pDNA condensation varied depending on dendrimer generation and PEGylation [dendrimer, nitrogen-to-phosphate ratio (N/P)]: [G2]-NH_2 (10/1), [G3]-NH_2 (2/1), PEG-[G2]-NH_2 (10/1), PEG-[G3]-NH_2 (5/1), and PEG-[G4]-NH_2 (10/1). Thus, G3 dendrimers were able to condense pDNA to a greater extent than G2 (Figure 5A) as previously observed for higher generations of PPI,[10] PLL,[32] and PAMAM.[42] This effect can be explained on the basis of the dendrimer−DNA interaction being predominantly of electrostatic nature and the higher surface charge of the larger dendrimers.[43] Interestingly, PEGylated dendrimers required higher amounts of polymer than their non-PEGylated counterparts to achieve complete condensation (Figure 5C). This effect, which had already been observed for numerous PEGylated cationic polymers, reflects the steric hindrance and shielding effect of the positive charges imposed by the PEG chains.[38,44,45] Surprisingly, to the best of our knowledge, the influence of PEG on the ability of dendritic block copolymers to condense pDNA has been sparingly studied to date.[32]

Gel electrophoresis and EB experiments also indicated a lower binding ability of PEG-[G4]-NH_2 than PEG-[G3]-NH_2 (Figures 4 and 5), an effect that may result from the higher hydrophobic character of the G4 dendritic block resulting in partial aggregation of PEG-[G4]-NH_2 in solution [according to photon correlation spectroscopy (PCS) experiments, data not shown] and hence in a lower effective concentration of amino groups ready for pDNA complexation.

3. Dendriplex Size. Irrespective of dendrimer generation and the presence/absence of PEG, GATG dendriplexes were in the nanometer scale as determined by PCS (Table 3 and Figure 6). Dendriplex size was not influenced by dendrimer generation, while PEGylation led to a significant increase in size. Dendriplexes of about 75 nm were obtained from [G2]-NH_2 and [G3]-NH_2 and of around 150 nm from the PEGylated dendrimers. Different N/P charge ratios were required for the various dendrimers to achieve a constant size: 10/1 for [G2]-NH_2, 2/1 for [G3]-NH_2, 10/1 for PEG-[G2]-NH_2, 5/1 for PEG-[G3]-NH_2, and 10/1 for PEG-[G4]-NH_2. These results are in accordance with the gel electrophoresis and EB assays and reflect the greater capacity of G3 and non-PEGylated dendrimers to condense pDNA. Indeed, the increase in size observed for the PEGylated dendriplexes is not unexpected as a result of the known interference of PEG chains

Table 3. Dendriplex Sizes (*z*-Average Values in nm) at Different N/P Charge Ratios[a]

	[G2]-NH_2		[G3]-NH_2		PEG-[G2]-NH_2		PEG-[G3]-NH_2		PEG-[G4]-NH_2	
charge ratio (N/P)	size (nm)	PI	size (nm)	PI	size (nm)	PI	size (nm)	PI	size (nm)	PI
2/1			86 ± 10	0.08−0.17						
5/1			76 ± 2	0.10−0.16			156 ± 3	0.34−0.40		
10/1	99 ± 16	0.11−0.25	73 ± 2	0.11−0.14	143 ± 7	0.25−0.36	161 ± 1	0.39−0.42	123 ± 5	0.16−0.23
20/1	74 ± 3	0.06−0.16	72 ± 2	0.11−0.18	153 ± 6	0.29−0.34	171 ± 5	0.41−0.43	132 ± 1	0.27−0.32
40/1	69 ± 4	0.10−0.18	81 ± 5	0.24−0.35	160 ± 5	0.24−0.30	197 ± 1	0.42−0.46	155 ± 5	0.47−0.49

[a] No data is given for charge ratios lower than required for complete pDNA complexation.

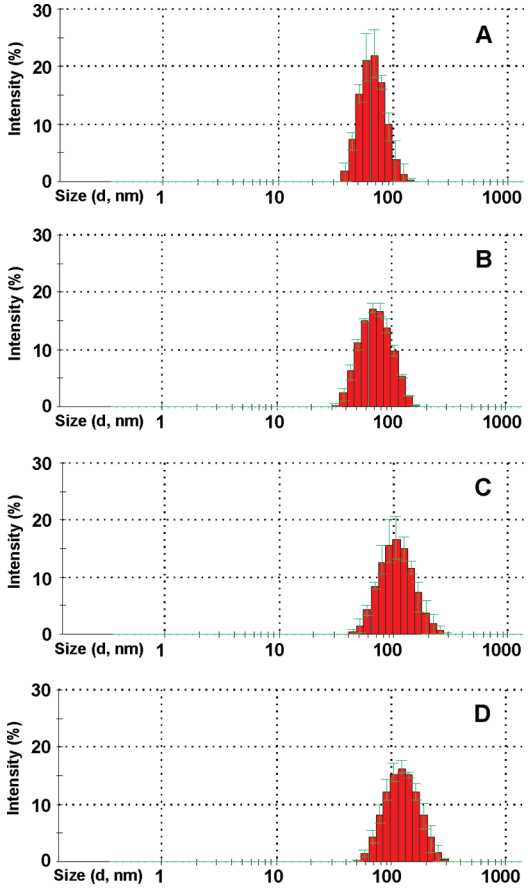

Figure 6. Size distribution (PCS) of the dendriplexes at the indicated N/P charge ratios: (A) [G2]-NH_2 at 20/1, (B) [G3]-NH_2 at 5/1, (C) PEG-[G2]-NH_2 at 10/1, (D) PEG-[G3]-NH_2 at 10/1.

with the formation of compact condensates[32,38,46−50] and the PEG creating a palisade around the particle.[51]

An interesting finding was that for N/P charge ratios above the characteristic value for each dendrimer the size of the resulting dendriplexes remained constant, while for lower N/P values, aggregates characterized by larger sizes resulted. This fact points out to dendriplexes as core−shell nanostructures with a core of dendrimers condensing a single pDNA and a dendritic shell surrounding this core, with the excess of dendrimers dissolved in the suspending medium (Figure 7).[52,53] This type of structure resembles very much that between nanoparticle *core substrates* that after being allowed to interact with an excess of a nanoscale *shell reagent* lead to core−shell nanostructures with reduced actual core valency. This phenomenon, which has been referred to as sterically induced stoichiometry (SIS),[54−56] has been claimed to control the dendronization of Au nanoparticles and quantum dots[57−59] and the preparation of tecto-dendrimers.[60,61]

In the present example, the relative size between the condensed pDNA core and the dendrimers at the shell would limit the number of the latter that may be accommodated on the core surface and force the excess of dendrimers to remain in solution (Figure 7). Interestingly, the much smaller size of the dendrimers compared to the core explains the insensitivity of the dendriplex size with generation. The SIS architecture is additionally supported by dendriplexes of around 150 nm being reported from alternative PEG−dendritic block copolymers incorporating PLL and PAMAM dendritic blocks.[34,62,63]

4. Surface Charge of Core−Shell Dendriplexes. The surface charge of the dendrimer−pDNA complexes was determined by laser Doppler anemometry (LDA, Figure 8). ξ-potential measurements give information about the surface properties of the carrier and thus about their molecular organization.

Negative values of ξ-potential were obtained for [G2]-NH_2 and [G3]-NH_2 aggregates at charge ratios below their characteristic threshold N/P for complete pDNA complexation. On increasing N/P, positive ξ potentials were obtained that reached a plateau at the charge ratio where all pDNA was complexed (2/1 for [G3]-NH_2, 10/1 for [G2]-NH_2) (Figure 8A). Further increases of N/P did not lead to variations in ξ-potential in agreement with the excess of dendrimers being dispersed in solution (see also section 3).

Interestingly, identical ξ-potential values were reached for [G2]-NH_2 and [G3]-NH_2. This reveals core−shell dendriplexes with similar positive charge and thus similar number of amino groups on the surface. Accordingly, and taking into account the 3^n multivalency of GATG dendrimers, on increasing the dendrimer generation from G2 to G3, a 3-fold lower concentration of shell dendrimers surrounding the pDNA core may be expected (Figure 7).

In SIS systems, the saturation number or maximum shell filling (N_{max}) can be predicted from the Mansfield−Tomalia−Rakesh equation, based on the relative radii between the *nanoparticle core* and *nanoscale shell reagent* (r_1 and r_2 respectively, Figure 7).[64] With the aim of determining the relative N_{max} for [G2]-NH_2 and [G3]-NH_2 dendriplexes, the hydrodynamic radii of these dendrimers (r_2) were calculated by means of ^{1}H PFG NMR experiments, using the Stejskal−Tanner and Stokes−Einstein equations (1.49 nm for [G2]-NH_2 and 2.38 nm for [G3]-NH_2, Table 1 and Figures 2, 3, and 7).

Indeed, by considering the *z*-average hydrodynamic radii of the core−shell dendriplexes ($R_h = r_1 + 2r_2$, see Figure 7) by PCS at a N/P 20 (37 nm for [G2]-NH_2 and 36 nm for [G3]-NH_2 dendriplexes, respectively; Table 3), the application of the Mansfield−Tomalia−Rakesh equation predicted a 2.85-fold reduction in N_{max} on going from [G2]-NH_2 to [G3]-NH_2. This value matches very well the 3-fold lower concentration of shell dendrimers expected for [G3]-NH_2 according to ξ-potential measurements and further supports the SIS nature of these dendriplexes.

As for the PEGylated dendriplexes, their surface charge was reduced when compared to the non-PEGylated ones. This is in agreement with previous reports for other PEGylated polycations and reflects the shielding effect of PEG

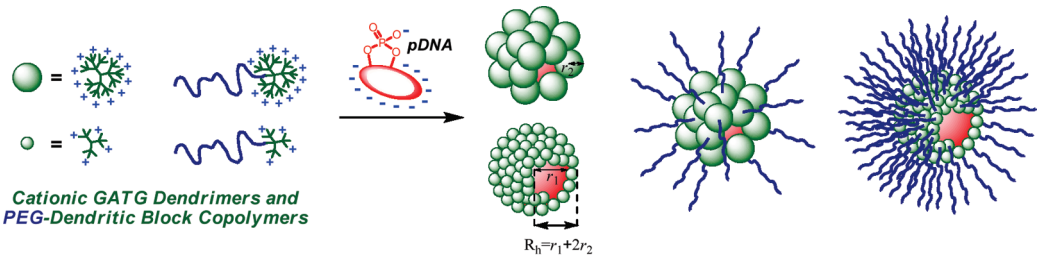

Mansfield-Tomalia-Rakesh Equation

$$N_{max}=\frac{2\pi}{\sqrt{3}}\left(\frac{r_1}{r_2}+1\right)^2$$

Radii (nm) and N_{max} values for dendriplexes

Dendriplex	R_h[a]	r_2[b]	r_1	N_{max}
G2	37	1.49	34.02	2060
G3	36	2.38	31.24	724

[a] Radii of dendriplexes determined by PCS.
[b] Radii of [Gn]-NH_2 determined by ^{1}H PFG NMR.

Figure 7. Schematic illustration of two generations of core−shell dendriplexes as SIS nanoarchitectures.

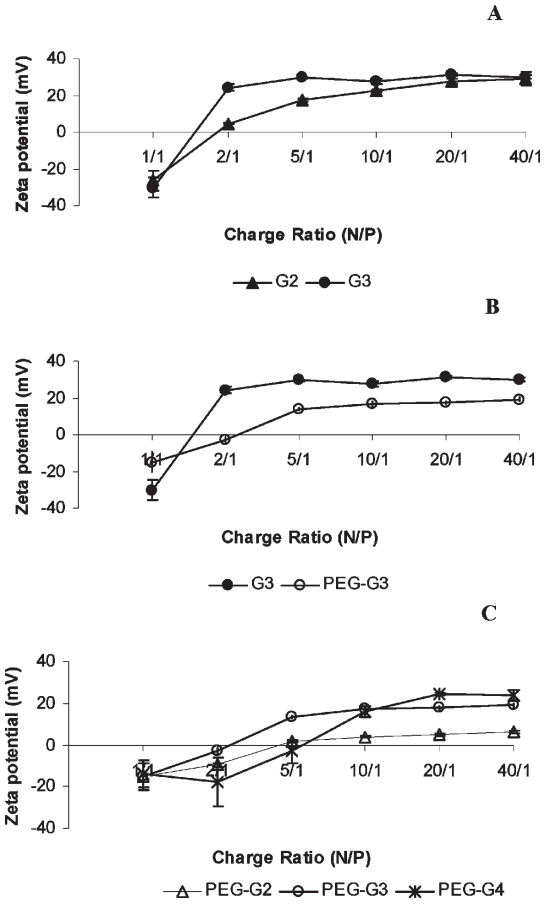

Figure 8. ξ-potential values for dendriplexes obtained from GATG dendrimers.

(Figure 8B).[32,38,65] Opposite to the non-PEGylated dendrimers, generation clearly affects the surface charge in this case, with lower generations leading to more effective charge shielding (Figure 8C). This generation-dependent charge neutralization can be explained again on the basis of the SIS nature of the core−shell dendriplexes, as an increased number of PEG−dendritic block copolymers of lower generation can be accommodated on the dendriplex core.

These results evidence the correlation between the architecture of the dendrimer and the surface charge of the dendriplex, an issue of special interest as surface charge determines the behavior of nanosystems within biological

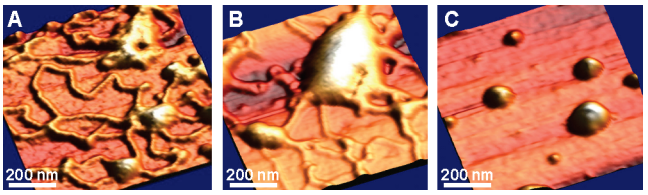

Figure 9. AFM images of naked pDNA (A) and dendriplexes with [G3]-NH_2 at N/P charge ratios 1/1 (B) and 5/1 (C).

media. Thus, positively charged polyplexes can interact with negatively charged cell membranes, facilitating the cellular uptake,[66] while for certain modalities of administration, including intravenous, neutral polyplexes are preferred to avoid interaction with blood cells.[30] Consequently, by selecting the dendritic architecture, it would possible to design dendriplexes for specific gene delivery applications, in what it could be considered as a sterically induced stealth stabilization.

5. Atomic Force Microscopy (AFM) Studies. It is known that during the formation of dendriplexes the characteristic extended structure of pDNA changes to a more compact one. In order to verify the assembly of pDNA with GATG dendrimers, dendriplex formation with [G3]-NH_2 was followed by AFM in tapping mode (Figure 9). Adsorbed plasmids became clearly visible when naked pDNA was deposited by drop-casting on freshly cleaved mica (Figure 9A). After incubation with [G3]-NH_2, partial complexation of pDNA was observed at a N/P ratio 1/1 (Figure 9B), which was complete and led to compact dendriplexes at a charge ratio 5/1 (Figure 9C). This results match previous observations in sections 2−4 and clearly confirm the ability of GATG dendrimers to bind and condense pDNA into well-defined structures.

6. Transmission Electron Microscopy (TEM) Studies. The influence of the dendrimer generation and the presence/absence of PEG on the morphology of the dendriplexes was studied by TEM. As seen in Figure 10, complexes showed compact structures, with PEG-[G2]-NH_2 being the only exception adopting a more extended morphology. Indeed, unpacked morphologies similar to the one of PEG-[G2]-NH_2 have been previously reported for polycationic systems with high PEG loadings,[46−48,50] including dendritic block copolymers,[32] and reflect the interference of PEG with the formation of compact condensates.[38,48,49] Interestingly, as the PEG fraction lowers on increasing the dendrimer generation, PEG-[G3]-NH_2 and PEG-[G4]-NH_2 resulted in more condensed structures.

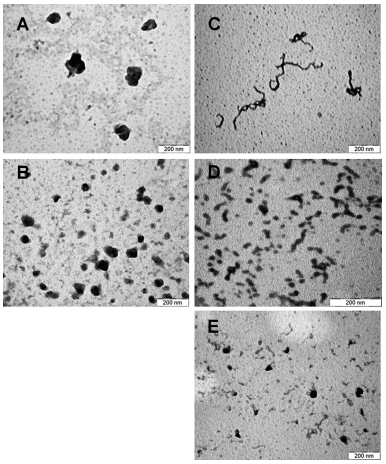

Figure 10. TEM images of dendriplexes (N/P: 40/1) from [G2]-NH_2 (A), [G3]-NH_2 (B), PEG-[G2]-NH_2 (C), PEG-[G3]-NH_2 (D), and PEG-[G4]-NH_2 (E).

Conclusion

The ability of amino-functionalized GATG dendrons and PEG−dendritic block copolymers to efficiently condense pDNA into well-defined core−shell dendriplexes has been demonstrated. The pDNA binding ability, dendriplex size, and surface charge of the resulting dendriplexes have been thoroughly investigated as a function of the dendritic architecture (generation and PEGylation). Dendriplexes have revealed as core−shell nanostructures with sterically induced stoichiometry, where the relative size between the condensed pDNA at the core and the shell dendrimers limits the core−shell stoichiometry by steric reasons. As a result, the surface charge of non-PEGylated dendriplexes revealed insensitive to generation, while a generation-dependent charge neutralization was observed for the PEGylated dendriplexes. The resulting sterically induced stealth stabilization offers a great opportunity for fine-tuning the requirements for specific gene therapy applications. Current work is aimed at investigating the influence of dendriplex structure on biological properties.

Acknowledgment. The authors gratefully acknowledge support from the Spanish Ministry of Science and Innovation (Refs SAF2004-09230-004-01, CTQ2006-12222/BQU, and CTQ2009-10963) and Xunta de Galicia (PGIDIT06PXIB209058PR). We thank Dr. R. Novoa-Carballal for help with the PFG NMR experiments. M. Raviña and A. Sousa-Herves also acknowledge fellowships received from the Spanish Government (FPI and FPU, respectively).

References and Notes

(1) Lou, D.; Saltzman, W. M. *Nature Biotechnol.* **2000**, *18*, 33–37.
(2) Guillot-Nieckowski, M.; Eisler, S.; Diederich, F. *New J. Chem.* **2007**, *31*, 1111–1127.
(3) Paleos, C. M.; Tsiourvas, D.; Sideratou, Z. *Mol. Pharmaceutics* **2007**, *4*, 169–188.
(4) Svenson, S.; Tomalia, D. A. *Adv. Drug Delivery Rev.* **2005**, *57*, 2106–2129.
(5) Dufes, C.; Uchegbu, I. F.; Schatzlein, A. G. *Adv. Drug Delivery Rev.* **2005**, *57*, 2177–2202.
(6) Raviña, M.; Paolicelli, P.; Seijo, B.; Sanchez, A. *Mini-Rev. Med. Chem.* **2010**, *10*, 73–86.
(7) Shcharbin, D.; Pedziwiatr, E.; Blasiak, J.; Bryszewska, M. *J. Controlled Release* **2010**, *141*, 110–127.
(8) Shcharbin, D.; Pedziwiatr, E.; Bryszewska, M. *J. Controlled Release* **2009**, *135*, 186–197.
(9) Kukowska-Latallo, J. F.; Bielinska, A. U.; Johnson, J.; Spindle, R.; Tomalia, D. A.; Baker, J. R., Jr. *Proc. Natl. Acad. Sci. U.S.A.* **1996**, *93*, 4897–4902.
(10) Zinselmeyer, B. H.; Mackay, S. P.; Schatzlein, A. G.; Uchegbu, I. F. *Pharm. Res.* **2002**, *19*, 960–967.
(11) Ohsaki, M.; Okuda, T.; Wada, A.; Hirayama, T.; Niidome, T.; Aoyagi, H. *Bioconjugate Chem.* **2002**, *13*, 510–517.
(12) Joester, D.; Losson, M.; Pugin, R.; Heinzelmann, H.; Walter, E.; Merkle, H. P.; Diederich, F. *Angew. Chem., Int. Ed.* **2003**, *42*, 1486–1490.
(13) Shah, D. S.; Sakthivel, T.; Toth, I.; Florence, A. T.; Wilderspin, A. F. *Int. J. Pharm.* **2000**, *208*, 41–48.
(14) Gillies, E. R.; Dy, E.; Fréchet, J. M. J.; Szoka, F. C. *Mol. Pharmaceutics* **2005**, *2*, 129–138.
(15) Gillies, E. R.; Fréchet, J. M. J. *J. Am. Chem. Soc.* **2002**, *124*, 14137–14146.
(16) Gitsov, I. *J. Polym. Sci., Part A: Polym. Chem.* **2008**, *46*, 5295–5314.
(17) Gitsov, I.; Hamzik, J.; Ryan, J.; Simonyan, A.; Nakas, J. P.; Omori, S.; Krastanov, A.; Cohen, T.; Tanenbaum, S. W. *Biomacromolecules* **2008**, *9*, 804–811.
(18) Gitsov, I.; Lambrych, K.; Lu, P.; Nakas, J.; Ryan, J.; Tanenbaum, S. W. In *Polymer Biocatalysis and Biomaterials*; Cheng, H. N., Gross, R. A., Eds.; ACS Symposyum Series; American Chemical Society: Washington DC, 2005; Vol. *900*, p 80.
(19) Gitsov, I.; Simonnyan, A.; Krastanov, A.; Tanenbaum, S. In *Polymer Biocatalysis and Biomaterials II*; Cheng, H. N., Gross, R. A., Eds.; ACS Symposyum Series; American Chemical Society: Washington DC, 2005; Vol. *999*, p 110.
(20) Fernandez-Megia, E.; Correa, J.; Riguera, R. *Biomacromolecules* **2006**, *7*, 3104–3111.
(21) Fernandez-Megia, E.; Correa, J.; Rodriguez-Meizoso, I.; Riguera, R. *Macromolecules* **2006**, *39*, 2113–2120.
(22) Munoz, E. M.; Correa, J.; Fernandez-Megia, E.; Riguera, R. *J. Am. Chem. Soc.* **2009**, *131*, 17765–17767.
(23) Sousa-Herves, A.; Fernandez-Megia, E.; Riguera, R. *Chem. Commun.* **2008**, 3136–3138.
(24) Novoa-Carballal, R.; Säwén, E.; Fernandez-Megia, E.; Correa, J.; Riguera, R.; Widmalm, G. *Phys. Chem. Chem. Phys.* **2010**, *12*, 6587–6589.
(25) Furgeson, D. Y.; Chan, W. S.; Yockman, J. W.; Kim, S. W. *Bioconjugate Chem.* **2003**, *14*, 840–847.
(26) Abbasi, M.; Uludag, H.; Incani, V.; Olson, C.; Lin, X.; Clements, B. A.; Rutkowski, D.; Ghahary, A.; Weinfeld, M. *Biomacromolecules* **2007**, *8*, 1059–1063.
(27) Takahashi, T.; Kono, K.; Itoh, T.; Emi, N.; Takagishi, T. *Bioconjugate Chem.* **2003**, *14*, 764–773.
(28) Kono, K.; Akiyama, H.; Takahashi, T.; Takagishi, T.; Harada, A. *Bioconjugate Chem.* **2005**, *16*, 208–214.
(29) Liu, W. G.; Zhang, X.; Sun, S. J.; Sun, G. J.; Yao, K. D. *Bioconjugate Chem.* **2003**, *14*, 782–789.
(30) Van Vlerken, L. E.; Vyas, T. K.; Amiji, M. M. *Pharm. Res.* **2007**, *24*, 1405–1414.
(31) Luo, D.; Haverstick, K.; Belcheva, N.; Han, E.; Saltzman, W. M. *Macromolecules* **2002**, *35*, 3456–3462.
(32) Mannisto, M.; Vanderkerken, S.; Toncheva, V.; Elomaa, M.; Ruponen, M.; Schacht, E.; Urtti, A. *J. Controlled Release* **2002**, *83*, 169–182.
(33) Merdan, T.; Kunath, K.; Petersen, H.; Bakowsky, U.; Voigt, K. H.; Kopecek, J.; Kissel, T. *Bioconjugate Chem.* **2005**, *16*, 785–792.
(34) Wood, K. C.; Little, S. R.; Langer, R.; Hammond, P. T. *Angew. Chem., Int. Ed.* **2005**, *44*, 6704–6708.
(35) Kim, T.-i.; Baek, J.-u.; Yoon, J. K.; Choi, J. S.; Kim, K.; Park, J.-s. *Bioconjugate Chem.* **2007**, *18*, 309–317.
(36) Kim, T.-i.; Seo, H. J.; Choi, J. S.; Jang, H.-S.; Baek, J.-u.; Kim, K.; Park, J.-S. *Biomacromolecules* **2004**, *5*, 2487–2492.
(37) Felgner, P. L.; Barenholz, Y.; Behr, J. P.; Cheng, S. H.; Cullis, P.; Huang, L.; Jessee, J. A.; Seymour, L.; Szoka, F.; Thierry, A. R.; Wagner, E.; Wu, G. *Hum. Gene Ther.* **1997**, *8*, 511–512.
(38) Petersen, H.; Fechner, P. M.; Martin, A. L.; Kunath, K.; Stolnik, S.; Roberts, C. J.; Fischer, D.; Davies, M. C.; Kissel, T. *Bioconjugate Chem.* **2002**, *13*, 845–854.
(39) Wu, D. H.; Chen, A. D.; Johnson, C. S. *J. Magn. Reson., Ser. A* **1995**, *115*, 260–264.
(40) Matsukawa, S.; Yasunaga, H.; Zhao, C.; Kuroki, S.; Kurosu, H.; Ando, I. *Prog. Polym. Sci.* **1999**, *24*, 995–1044.
(41) Lepecq, J.-B.; Paoletti, C. *J. Mol. Biol.* **1967**, *27*, 87–106.
(42) Bielinska, A. U.; Chen, C.; Johnson, J.; Baker, J. R., Jr. *Bioconjugate Chem.* **1999**, *10*, 843–850.
(43) Tomalia, D. A.; Naylor, A. M.; Goddard, W. A., III *Angew. Chem., Int. Ed.* **1990**, *29*, 138–175.
(44) Lin, S.; Du, F.; Wang, Y.; Ji, S.; Liang, D.; Yu, L.; Li, Z. *Biomacromolecules* **2008**, *9*, 109–115.

(45) Toncheva, V.; Wolfert, M. A.; Dash, P. R.; Oupicky, D.; Ulbrich, K.; Seymour, L. W.; Schacht, E. H. *Biochim. Biophys. Acta* **1998**, *1380*, 354–368.
(46) Kwoh, D. Y.; Coffin, C. C.; Lollo, C. P.; Jovenal, J.; Banaszczyk, M. G.; Mullen, P.; Phillips, A.; Amini, A.; Fabrycki, J.; Bartholomew, R. M.; Brostoff, S. W.; Carlo, D. J. *Biochim. Biophys. Acta* **1999**, *1444*, 171–190.
(47) Rackstraw, B. J.; Martin, A. L.; Stolnik, S.; Roberts, C. J.; Garnett, M. C.; Davies, M. C.; Tendler, S. J. B. *Langmuir* **2001**, *17*, 3185–3193.
(48) Rackstraw, B. J.; Stolnik, S.; Davis, S. S.; Bignotti, F.; Garnett, M. C. *Biochim. Biophys. Acta* **2002**, *1576*, 269–286.
(49) Remaut, K.; Lucas, B.; Raemdonck, K.; Braeckmans, K.; Demeester, J.; De Smedt, S. C. *Biomacromolecules* **2007**, *8*, 1333–1340.
(50) Wolfert, M. A.; Schacht, E. H.; Toncheva, V.; Ulbrich, K.; Nazarova, O.; Seymour, L. W. *Hum. Gene Ther.* **1996**, *7*, 2123–2133.
(51) Putnam, D.; Zelikin, A. N.; Izumrudov, V. A.; Langer, R. *Biomaterials* **2003**, *24*, 4425–4433.
(52) Orberg, M. L.; Schillen, K.; Nylander, T. *Biomacromolecules* **2007**, *8*, 1557–1563.
(53) Storkle, D.; Duschner, S.; Heimann, N.; Maskos, M.; Schmidt, M. *Macromolecules* **2007**, *40*, 7998–8006.
(54) Tomalia, D. A. *Prog. Polym. Sci.* **2005**, *30*, 294–324.
(55) Tomalia, D. A. *J. Nanopart. Res.* **2009**, *11*, 1251–1310.
(56) Tomalia, D. A. *Soft Matter* **2010**, *6*, 456–474.
(57) Gopidas, K. R.; Whitesell, J. K.; Fox, M. A. *J. Am. Chem. Soc.* **2003**, *125*, 14168–14180.
(58) Guo, W.; Li, J. J.; Wang, Y. A.; Peng, X. *J. Am. Chem. Soc.* **2003**, *125*, 3901–3909.
(59) Love, C. S.; Chechik, V.; Smith, D. K.; Brennan, C. *J. Mater. Chem.* **2004**, *14*, 919–923.
(60) Tomioka, N.; Takasu, D.; Takahashi, T.; Aida, T. *Angew. Chem., Int. Ed.* **1998**, *37*, 1531–1534.
(61) Uppuluri, S.; Swanson, D. R.; Piehler, L. T.; Li, J.; Hagnauer, G. L.; Tomalia, D. A. *Adv. Mater.* **2000**, *12*, 796–800.
(62) Choi, J. S.; Choi, Y. H.; Park, J. S. *Bull. Korean Chem. Soc.* **2004**, *25*, 1025–1030.
(63) Kim, T.-i.; Jang, H.-s.; Joo, D. K.; Choi, J. S.; Park, J.-S. *Bull. Korean Chem. Soc.* **2003**, *24*, 123–125.
(64) Mansfield, M. L.; Rakesh, L.; Tomalia, D. A. *J. Chem. Phys.* **1996**, *105*, 3245–3249.
(65) Zhang, X.; Pan, S.-R.; Hu, H.-M.; Wu, G.-F.; Feng, M.; Zhang, W.; Luo, X. *J. Biomed. Mater. Res., Part A* **2008**, *84*, 795–804.
(66) Boussif, O.; LezoualC'H, F.; Zanta, M. A.; Mergny, M. D.; Scherman, D.; Demeneix, B.; Behr, J.-P. *Proc. Natl. Acad. Sci. U.S.A.* **1995**, *92*, 7297–7301.